Article

Implications of Geometry and the Theorem of Gauss on Newtonian Gravitational Systems and a Caveat Regarding Poisson's Equation

Anne M. Hofmeister * and Robert E. Criss

Department of Earth and Planetary Science, Washington University, St. Louis, MO 63130, USA; criss@wustl.edu
* Correspondence: hofmeist@wustl.edu; Tel.: +1-314-935-7440

Abstract: Galactic mass consistent with luminous mass is obtained by fitting rotation curves (RC = tangential velocities vs. equatorial radius r) using Newtonian force models, or can be unambiguously calculated from RC data using a model based on spin. In contrast, mass exceeding luminous mass is obtained from multi-parameter fits using potentials associated with test particles orbiting in a disk around a central mass. To understand this disparity, we explore the premises of these mainstream disk potential models utilizing the theorem of Gauss, thermodynamic concepts of Gibbs, the findings of Newton and Maclaurin, and well-established techniques and results from analytical mathematics. Mainstream models assume that galactic density in the axial (z) and r directions varies independently: we show that this is untrue for self-gravitating objects. Mathematics and thermodynamic principles each show that modifying Poisson's equation by summing densities is in error. Neither do mainstream models differentiate between interior and exterior potentials, which is required by potential theory and has been recognized in seminal astronomical literature. The theorem of Gauss shows that: (1) density in Poisson's equation must be averaged over the interior volume; (2) logarithmic gravitational potentials implicitly assume that mass forms a long, line source along the z axis, unlike any astronomical object; and (3) gravitational stability for three-dimensional shapes is limited to oblate spheroids or extremely tall cylinders, whereas other shapes are prone to collapse. Our findings suggest a mechanism for the formation of the flattened Solar System and of spiral galaxies from gas clouds. The theorem of Gauss offers many advantages over Poisson's equation in analyzing astronomical problems because mass, not density, is the key parameter.

Keywords: theorem of Gauss; Poisson's equation; self-potential; instability; symmetry; geometry

1. Introduction

Constraints imposed by initial or boundary conditions under any given law of physics provide a framework that dictates the form of the appropriate mathematical solution. Unfortunately, simplifying assumptions in models can negate this essential connection. The geometrical nature of boundary conditions permits quantitative evaluation. For example, permissible periodic vibrations of molecules and crystalline solids are restricted by symmetry constraints imposed by group theory [1]. Because harmonic oscillations are related to circular orbits [2], symmetry can be likewise used to evaluate orbital models. Furthermore, shape being related to symmetry permits qualitative evaluation through visualization.

Newton's law is spherically symmetric: yet, axisymmetric disk geometry is currently assumed in most models of the periodic, circular, rotational motions observed for gravitationally-bound galactic interiors, e.g., [3–8]. The coin shape has been the focus in galactic dynamics since 1964 [3] after Perek [9] declared, without proof and erroneously [10], that density (ρ) variations in the oblate spheroid shape required for spinning bodies [11] are independent in the z and r directions (the vertical distance along

the special axis and the equatorial radius, respectively). Vertical and radial variations in density are also linked in disk geometries through the total mass. The effects of these mathematical links on mass models have not been explored.

The view that huge halos of dark matter surround galaxies [12,13] arises from multicomponent fitting models of their tangential velocities (*v*) as a function of *r* that are obtained through Doppler measurements and are known as RC, rotation curves, e.g., [3–5]. Early work was based on the reduced two-body problem (Keplerian orbits), whereas more recent studies superimpose solutions to Poisson's equation for orbiting test particles [3,5–8]. Yet, decades of searches have not detected these presumably non-baryonic entities [14,15]. Multicomponent mass models are characterized by ambiguities (trade-offs), as is well-known, e.g., [16,17], and provide huge proportions of non-baryonic matter (75–99.9% of total galactic mass [7,18]) that exceed cosmological estimates of ~26% [19]. The smaller excess of three-times the luminous mass is associated with large spirals, whereas the huge excess is associated with dwarf spheroidal galaxies. Use of 4 to ~9 parameters (e.g., [7,8,16,20]) to explain a single measured quantity (*v*) shows that mass models are under-constrained [21]. Ambiguities arise because parameters are multiplied [22]. The above situation has motivated many researchers (see [23]) to consider modifications to Newton's law, after Milgrom [24], whereas a few studies have explored relativistic effects [15,25]. Under non-Newtonian physics, dark matter is not needed to explain *v*(*r*) data for diverse types of galaxies. However, these systems are slowly rotating, so one might conclude that non-Newtonian effects should involve perturbations, as exemplified by the effect of relativity on Mercury's orbit [26], rather than grossly altering the tie of calculated mass to rotational motions.

The lack of direct evidence for dark matter has recently motivated computationally-intensive force calculations [27–29] as an alternative to using Poisson's equation, which has dominated mass models for the past ~20 years [30]. These three independent studies using force calculations have shown that non-baryonic matter is negligible for certain density distributions. Importantly, Feng and Gallo [27] showed that the force at any given radius is derived from mass both inside and outside this radius.

Additionally, early measurements of RC showed that the interior parts of spiral galaxies spin like solid bodies, but this behavior is not explained by traditional orbital models [5]. An object does not need to be solid to spin, as exemplified by hurricanes (Figure 1). Atmospheric cyclones have smaller length- and time-scales and involve different forces than self-gravitating galaxies, yet their images and rotation curves strongly resemble those of spiral galaxies. This observation is congruous with the view long ago [31] that galactic motions are internally organized and represent spin of the entire object. This view motivated many studies of the dynamics of the oblate spheroid, e.g., [3].

Internal organization is a consequence of interactions existing between galactic constituents: such interactions have been documented in force models [27–29]. The above led us to model spiral galaxies as spinning entities [10]. Our Newtonian model with varying internal density provides mass *M* at the visible edge of a coherently spinning galaxy as:

$$M_{\text{edge}} = v_{\text{edge}}^2 \frac{2}{3} \left(\frac{5-n}{5} \right)^3 \frac{r_{\text{edge}}}{G} \frac{e}{\arcsin(e)} \tag{1}$$

where *G* is the gravitational constant, *e* is ellipticity, and a polytropic density distribution is assumed. Using an index *n* = 2, which averages the indices of H and H_2 gas [32], provides a gravitational mass that linearly correlates with galactic luminosity for 14 well-characterized spirals [10]. No fitting parameters are needed, but the aspect ratio is required to compute *e* (see Sections 2.2 and 2.7).
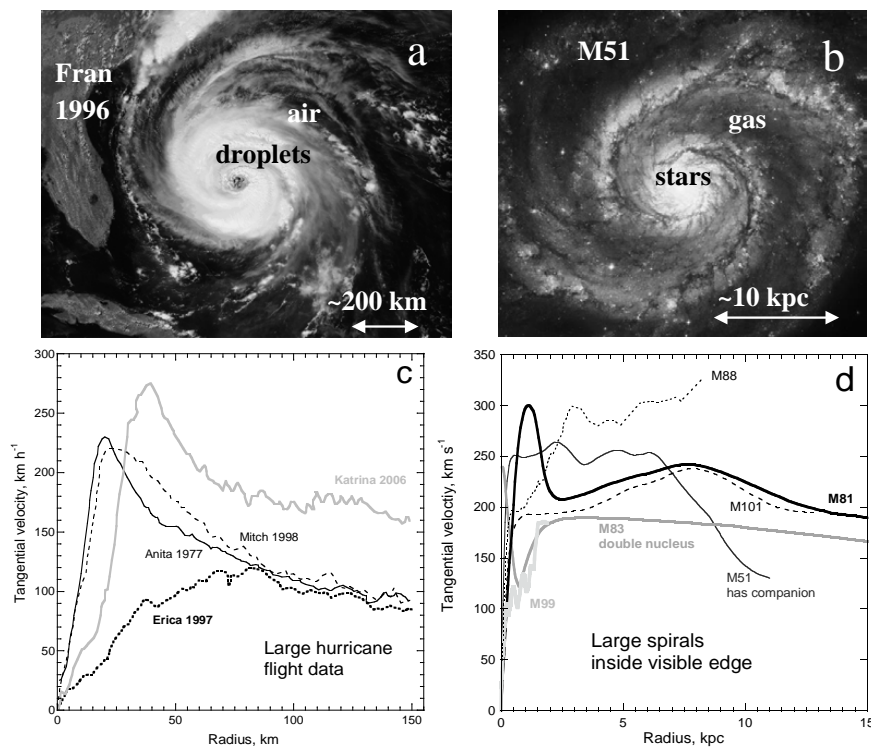
Figure 1. Comparison of hurricanes to spiral galaxies. (**a**) Image of Category 3 Fran off the Florida coast. See https://www.weather.gov/ilm/HurricaneFran for time-lapse images and maps of wind speed. (**b**) Image of the Whirlpool galaxy from NASA/IPAC Extragalactic Database (NED) [33] Both images are in the visible, public domain and were accessed in July 2017. Scale bars are approximate. (**c**) Rotation curves of four large hurricanes, similar to Fran, from flight data. Data sources are [34,35]. For images, see http://www.noaa.gov/ from the National Oceanic and Atmospheric Administration. Note that the hurricane data focus on the central regions. (**d**) Rotation curves of complex spirals. Data sources are [36,37]. These data focus on the areas far from galactic centers. Hurricanes and spiral galaxies have null central velocities, as required for spin.

Because force calculations and spin models both point to galactic mass being baryonic, it is worth investigating the mathematical constructs of mainstream RC models: these utilize Poisson's equation under the assumption that obits of test particles describe rotation curves. Our concern is the possible existence of systematic errors, which can only be evaluated through analytical mathematics and physical principles.

Evaluating RC models requires delving into geometry, because shape and symmetry govern the moment of inertia, which is key to quantifying kinetic energy, angular momentum, torque, work and power [2]. We exploit the theorem of Gauss and find that unrecognized stipulations exist on density in mainstream models. This mathematical result is important due to wide-spread use of Poisson's equation. Moreover, the theorem of Gauss offers a great advantage due to its dependence on interior mass, which is directly tied to the total energy stored in the motions of the constituent stars and gas. Furthermore, fewer integrations are required, which reduces uncertainties.

This paper focuses on the mathematical physics of self-gravitating objects. For the prevalent numerical calculations to be correct, the underlying analytical equations must be valid. Another numerical study that involves fitting data cannot resolve the issues discussed above. Instead, the need is to carefully examine the analytical formulae on which mainstream models are based. Section 2 provides background material. This includes calculating the mass for all 356 galaxies for which data exist on both RC and luminosity, using our spin model of (1). Section 3 explores problems arising in applying Poisson's equation, based on mathematics and physics books. Section 4 uses

the theorem of Gauss to estimate vertical gravitational instability of popular cylindrical geometries. Section 5 applies our mathematical results to the formation of the Solar System from a dusty nebula, based on [38,39]. Differential spin is explored in a companion paper [40], which derives the interior potential for nested homeoidal shells and determines $\rho(r)$ from $v(r)$ and the aspect ratio only for 51 galaxies. Another paper derives exterior potentials for oblate spheroids with varying internal density, provides numerical confirmation and applies these to planets [41].

2. Implications of Geometry on Internal Motions of Spiral Galaxies

2.1. Background: Synopsis of RC Models

Existing RC models use the cylindrical coordinate system, which is a likely source of problems. The term "thick disk" is used to describe galaxy geometry, meaning a coin shape or a short cylinder; whereas "thin disk" is used to describe the concentration of matter in the equatorial plane. In actuality, the z-dependence is not used to fit v because v is determined as a function of r only from the Doppler measurements. The obvious reason is circular motions are assumed in order to analyze the Doppler data, which are a two-dimensional projection of motions in three-dimensions.

The physical picture in available RC disk mass models is that of orbiting test masses (Figure 2a). Early studies, which are the basis of all models [6], assume that the gravitational and centrifugal forces balance (Section 2.5). A modification of Poisson's equation (after [30]) is currently used to provide the gravitational potential for an axially symmetric, but non-spherical shape assuming various density distributions, and this result is used to ascertain v through a force balance. A few models begin by assuming a logarithmic form for the potential [6].
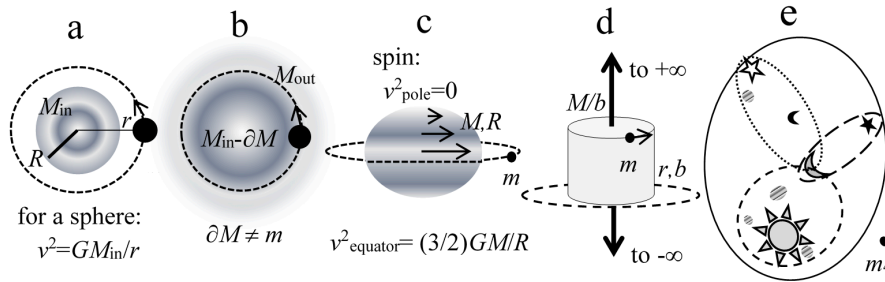
Figure 2. Configurations relevant to rotational motions of spiral galaxies. (**a**) View down the z axis of a satellite (black dot, mass m) orbiting outside an axisymmetric body with mass M and body radius R that is smaller than the orbital radius r. The Keplerian orbital velocity equation listed presumes a spherical body, resulting in the independence of v on m. (**b**) View down the z axis of a satellite orbiting inside a gassy body. The satellite displaces a volume of gas at r corresponding to mass ∂M, but need not have this exact mass or corresponding ρ. Orbits are also Keplerian if the body is spherically symmetric and the satellite is relatively small, because the spherical mass outside the orbit (M_{out}) does not have an effect, presuming small m that negligibly perturbs the system. (**c**) Side view of a satellite orbiting a large, spinning body with oblate symmetry and homogenous density. Equatorial spin (from the Virial theorem [39]) exceeds that of a Keplerian orbit, whereas the poles are stationary, showing that rotational energies are distributed differently in spin than in orbits. (**d**) Schematic for application of the theorem of Gauss to an orbit of a satellite m at radius r about an infinite line (heavy arrows) with a given linear density. Height b from the equatorial plane (dotted curve) is immaterial, which shows that the orbits define hollow cylinders. (**e**) Schematic illustrating that different formulations are needed for masses inside vs. outside of a boundary. The dashed line represents the volume used to ascertain the force on some moon due to its proximal sun and planets. Additional forces from more distant star systems are computed using the dotted and long-dashed line enclosures. If the force on distant mass m_4 is computed for all stars and planets, which requires the solid perimeter, then the mass of the moon is part of the interior mass.

2.2. Background: The Equilibrium Shape of Rotating, Gravitating Objects under Newtonian Physics

Newton and Maclaurin showed that the oblate spheroid was the equilibrium shape of a large, spinning, gravitational body [11]. Their force balance is in reference to the non-spinning sphere being in equilibrium. This oblate shape has been confirmed for the Earth, despite the presence of additional forces associated with tidal friction and solid body deformation, which were not accounted for by Newton or Maclaurin. This shape is furthermore evident in images of the Sun and gas giants. Although the triaxial ellipsoidal shapes of Jacobi are permissible [42], the ostensibly circular motions in spiral galaxies indicate the higher symmetry of the oblate suffices.

The geometry of an oblate spheroid (Figure 2c) is described by the ellipticity (*e*), which relates the minor axis (*c*) to the major (*a*):

$$e = \left(1 - c^2/a^2\right)^{1/2} \tag{2}$$

When *e* = 0, the object is a sphere. When *e* = 1, the object is a discoid with no thickness that extends to infinity. The latter differs substantial from disk geometry and cannot rotate because an object with finite mass, finite ω and infinite radius would possess infinite rotational energy. Hence, rotation at the limit *e* = 1 is disallowed.

2.3. Perek's Error

Historic deductions that galaxies have spheroidal shapes [31] have been subsequently confirmed by images and light contours at wavelengths from the visible to radio (Figure 3; [20,33,43]). However, because formulae for attraction of an exterior test point to the oblate spheroid in cylindrical coordinates are complicated [44] and because RC data only provide the radial component, Perek's [9] declaration that density in the *z* direction is independent of that in the *r* direction was incorporated in modelling circa 1964.
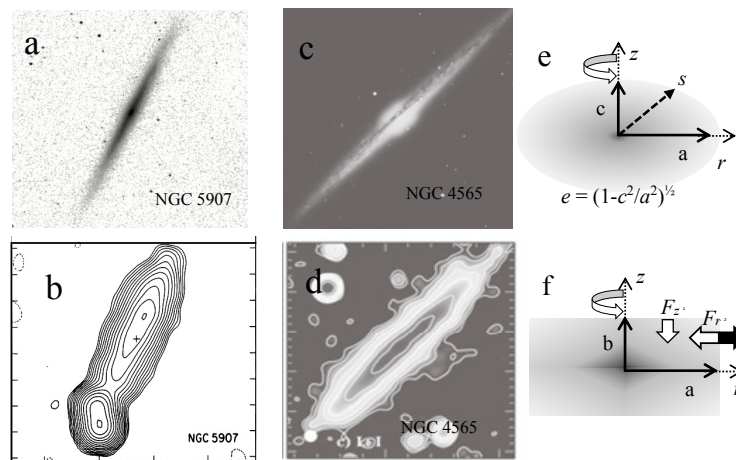

Figure 3. Galactic images and intensity contours of edge-on spiral galaxies at four different wavelengths and schematics of relevant geometries, confirming that the 3D shapes of these objects are approximated by the oblate spheroid. Spiral galaxy shapes face-on are roughly circular (not shown). (**a**) Image at IR wavelengths (λ = 1.6 μm) of edge-on spiral galaxy NGC 5907. (**b**) Contours of light for NGC 5907 (on a similar scale as the image), but emitted at λ = 21 cm, which monitors H gas. (**c**) Image in the visible of edge-on spiral galaxy NGC 4565. (**d**) Contours of NGC 4565 at radio wavelengths, λ = 5 cm, on a similar scale from [43]. Other panels from [33]: all images are public domain. (**e**) Schematic *r-z* cross-section of a containerless oblate spheroid with gradational density. The density contours are mathematically similar to the object shape. (**f**) Schematic *r-z* cross-section of a containerless disk with gradational density, showing perpendicular gravitational forces, *F* (white arrows), and the centripetal force (black arrow). To differentiate the disk from a discoid, the vertical disk height is designated as "b". For a central concentration, the density contours may differ from the shape of the coordinate system, as indicated.

Yet, Newton demonstrated that spinning homeoids (nested shells, which assemble to form the spheroid; Figure 4a,b) are equipotential. An equipotential surface necessarily has constant density; otherwise, the excess density regions would create an unbalanced force along the surface. Because the surface has constant ρ, variations in ρ with z depend on variations with r, as follows:

The definition for the oblate spheroid surface (an ellipse in profile) can be used to relate z to r for each surface of the nested homeoids (Figures 3e and 4b), all of which must have the same ellipticity:

$$z^2 = \left(1 - e^2\right)\left(a^2 - r^2\right) \tag{3}$$

From (3), density perpendicular to the equatorial plane is regulated by the flattening, the exterior radius of the body and the functionality of $\rho(r)$, and therefore, $\rho(z)$ depends on $\rho(r)$ for oblate spheroids. This situation occurs because the oblate is simply a flattened sphere, and so, the only variable is the equatorial radius r, which is related to s, the radius in spherical coordinates.

The additional parameter used to describe $\rho(z)$ imparts a degree of freedom to RC models, which is not present in a self-gravitating system. Consequently, the fits may not necessarily describe the gravitational mass.
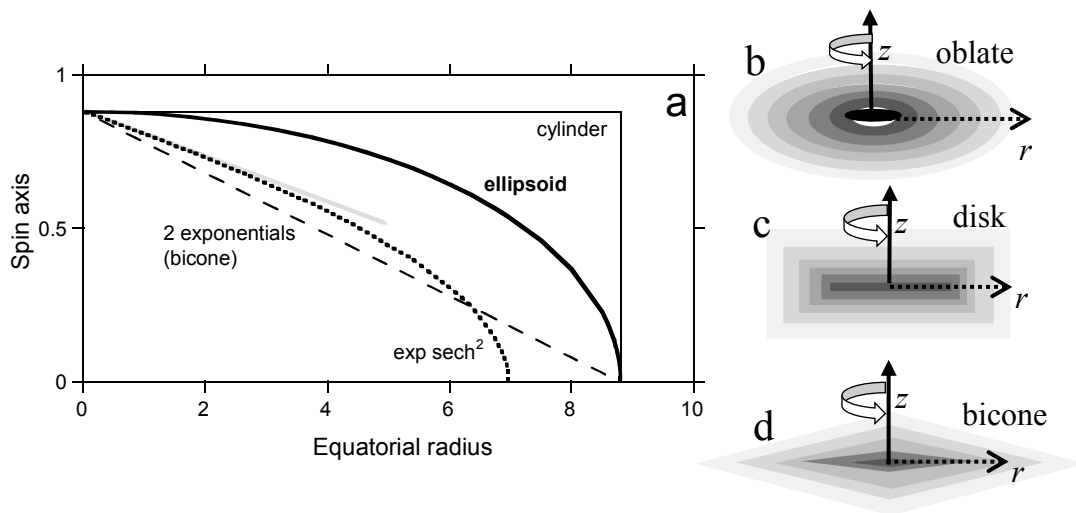

Figure 4. Surfaces and shapes considered for spiral galaxies in previous literature. (**a**) Mathematically exact cross-sections in the *r-z* plane for the four relevant geometries from Equations (3)–(6). Constants were set so that all shapes have the same *z* intercept and the same *b:a* or *c:a* ratio of 1:10. Grey line = slope at apex for Equation (6). (**b–d**) Schematics of density variations in the *r-z* plane for three shapes, using discrete nested layers for visualization of the internal structure, which is actually gradational. Nesting is schematic only. Not shown is the shape associated with the $\exp(-r/a)\,\text{sech}^2(z/b)$ density function (6), which would have pointy apexes, like the bicone, but rounded sides, like the oblate spheroid.

2.4. Shape Is Defined by Isodensity Surfaces, Not by the Coordinate System

If a liquid or gas is held within some container, its walls define the surface of the object, and the density of the material is referenced to the coordinate system appropriate for the shape of the container. Rainclouds and astronomical objects have no containing walls, and hence, their surfaces (and shapes) are defined by density contours (and measured by light contours, e.g., [20,43]).

In RC models, two density functions are assumed for the two directions, most commonly an exponential in *r* and either an exponential or a sech squared function in *z*. These functions originate in fitting luminosity data of the brighter inner portions of galaxies [45,46] and do not describe the outer regions where RC data are collected (e.g., [3–5]). Measurements of vertical velocities and

luminosities are difficult, due to flat geometry of spirals, so the dependence of these variables on z is generally unconstrained.

Regarding the double exponential,

$$\rho(r,z) = \rho_0 e^{(-r/a)} e^{(-|z|/b)}, \tag{4}$$

(e.g., [47]) the surface profile in each quadrant of the *r-z* plane is defined by equations such as:

$$\frac{r}{a} + \frac{z}{b} = \text{constant} \tag{5}$$

which is a straight line in this plane (Figure 4a). Combining all quadrants yields a bicone (Figure 4d). For:

$$\rho(r,z) = \rho_0 e^{(-r/a)} \text{sech}^2(z/b), \tag{6}$$

(e.g., [48]) using the contour plot function of Mathematica gives the profile in Figure 4a, which upon rotation about *z* and reflection about the equatorial plane gives a bi-mosque top (not shown). Figure 4 shows that these contour types differ from the rectangular cross-section of cylindrical geometry. Furthermore, the assumed shape clearly differs from galactic images (Figure 3), which closely resemble the ellipsoidal cross-section associated with the equilibrium, spinning Newtonian shape.

Assembly of 3D objects from density profiles in RC models are sketched in Figure 4b–d, where we have represented density gradations through discretization. Cylinder shapes are comprised of nested hollow pillboxes with corners, whereas density functions of both (4) and (6) require pointy apexes. Therefore, the geometrical constructs of RC models have unrealistic discontinuities that do not occur in galaxies. Instead, galaxies are reasonably represented by the expected equilibrium oblate spheroid with its continuous and smooth surfaces (Figure 3a–e; diverse images of edge-on spiral galaxies are available on the web [33]).

By assuming particular density functions, RC models automatically assume a specific object shape. An unrecognized problem is that the functions used provide shapes different from the coin-like shape (Figure 4). Because measurements do not constrain the *z* dependence of ρ and because RC models err in other ways (below and Section 3), we do not further explore this issue of the assumed shape being inconsistent with both the assumed density and the expected equilibrium shape.

2.5. Assumptions Underlying Depiction of RC as Orbits of Test Particles

Mainstream efforts model orbits of a test mass about the object [49,50]. Hence, efforts have been directed to explain why the observed orbits are not Keplerian, which requires:

$$v^2(r) = \frac{G \sum M_{in,i}(r)}{r} \tag{7}$$

where M_{in} is the interior mass for different constituents or components in the galaxy (i.e., stars, gas, bulge, disk, halo, black hole). Equation (7) results from balancing gravitational and centrifugal forces and defines the dynamical mass $M_{dynamic} \equiv \Sigma M_{in}$ up to some large *r* where velocity measurements terminate [33,51].

For (7) to be exact, many unrealizable conditions must be met, which stem from geometry (Figure 2).

- The interior mass must be spherically distributed, and not spinning, or it would be oblate.
- The orbital radius *r* must exceed the radius *r* used to compute mass, if only by a small amount (δr).
- If the satellite is sufficiently far from the galaxy (Figure 2a) for the point mass approximation to be valid, then details concerning the shape and density of the galactic interior are immaterial. Although a sufficiently distant satellite would constrain the total galactic mass, available data for extreme distances where the point mass approximation is valid are only possibly met for the

Milky Way and Andromeda (Figure 5). However, their proximity alters orbits of their satellites from Keplerian.

- If the satellite is located in the interior (Figure 2b), then it can be approximated as displacing an element in the galaxy. For large *r*, this approximation should be reasonable because the effect on displacing interior mass is small. However, for (7) to hold requires that M_{out} is distributed in a spherically-symmetric manner, so that it does not affect interior orbits.

- Because the test mass (*m*) is not part of (7), the mass or density exactly at *r* is unconstrained in the orbital picture of either Figure 2a or Figure 2b. It has long been known that orbits constrain mass of the central object, but not of the satellites, e.g., [2].

- Importantly, (7) is based on the moment of inertia equaling mr^2, which describes a point mass, a ring, or a hollow cylinder with open ends (Table 1). This moment does not equal that of any closed 3D shell, including spherical shells and homeoids [40], or the bicone shell (Table 1).

Table 1. Moments of inertia about the polar (*z*) axis for homogeneous density.

Shape	I, Solid Body	I, Shell	Definition of R
bicone	$3/10\, MR^2$	$1/2\, mR^2$	cone base radius
sphere	$2/5\, MR^2$	$2/3\, mR^2$	body radius
oblate	$2/5\, MR^2$	$2/3\, mR^2$	equatorial radius
cylinder or disk	$1/2\, MR^2$	mR^2 (open ends)	body radius
box (square ends)	$2/3\, MR^2$	$4/3\, mR^2$ (open ends)	$1/2$ edge
thin ring or point	-	mR^2	radius

Notes: For the shells, ∂m rather than *m* should be used in the integration. Formulae are from [2] or were obtained by integration or differentiation.

Using Poisson's equation to provide M_{in} does not remedy the above problems because it also describes orbits of test particles [49,50] and therefore implicitly assumes $I = mr^2$, which is unconnected with that of closed three-dimensional shells or shapes (Table 1). Additional issues exist (Section 3).
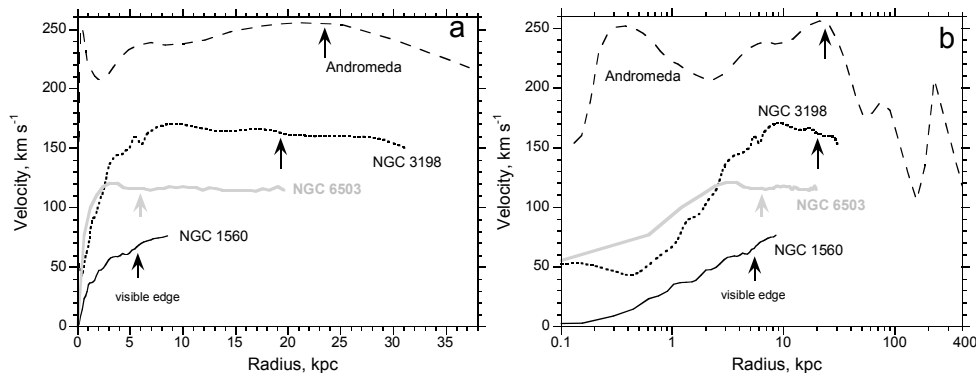

Figure 5. Representative rotation curves of spiral galaxies. (**a**) Linear plot at low radius. (**b**) Logarithmic plot to very high *r*. For both panels: the visible edge (arrows) is determined from isophotes (see the NED website [33]). Andromeda is close, permitting measurement at a great distance from its center. However, *r* = 400 kpc lies midway between the centers of the Milky Way and Andromeda. Data on Andromeda compiled by Sofue [7]. Data on the other galaxies are from the compilation of Bottema and Pestano [8] who considered these rotation curves (RC) to be collected under optimal conditions. The three galaxies shown have RC similar to the archetypes of non-interacting galaxies [51], where velocities most typically increase with *r* and then become flat. The decrease of *v* with *r* at large *r* for Andromeda and NGC 3198 exists in more distant galaxies, but is far less common than the patterns of NGC 1560 or 6503.

2.6. Shape and Spin

Centers of spiral galaxies spin like tops (~constant angular velocity, $\omega = v/r$), as shown in Figures 1 and 5. This key feature cannot be explained by the orbital picture [5], although fits can reproduce this trend with r, through the use of multiple parameters and trade-offs. As r increases past the central region, the observed dependence of v on r first becomes weaker than linear, then approaches a constant at large r, and in the few studies conducted at very large r, v decreases as r increases further (Figure 5). This observed behavior suggests that galaxies should be treated as spinning objects in which internal coherency decreases with radius and in which the dynamics grade from spin of a top into orbits of distant satellites around the spinning top [10].

The importance of shape to a spinning object, which is described by symmetry elements in group theory, cannot be overemphasized. Shape governs both the moment of inertia and gravitational potential, which respectively are:

$$I = \int_0^M s^2 \cos^2 \varphi \, dm; \ I_{\text{sphere}} = \frac{2}{3} \int_0^S 4\pi s^4 \rho(s) ds \tag{8}$$

$$U_{\text{g,self,sphere}} = -\int_0^M G\frac{M_{\text{in}}}{S} dm = \int_0^S G\left[\int_0^S 4\pi f^2 \rho(f) df \right] 4\pi s \rho(s) ds \tag{9}$$

where ϕ is the angle from the equatorial plane (towards the z axis). The relevance of the self-gravitational potential to spin is discussed in [39] and Section 3.2. To illustrate the effect of shape, Table 1 lists values for I for homogeneous density shapes and shells. For very complicated shapes, see [52].

The ratio of the gravitational potential of a sphere to any other shape does not equal the ratio between their moments of inertia. Hence, the energetics of spin depend strongly on symmetry and shape. Companion papers provide models of spin for oblate spheroid shapes considering internally-varying density for solid bodies [10] and for differentially-rotating bodies [40].

2.7. Mass Associated with Spin and Why This Differs from Mass Based on Orbiting Test Particles

Figure 2 encapsulates why different masses are obtained from spin and orbital models. The simple equations in Figure 2ac for solid bodies provide a total mass for a spinning object that is 2/3 that of the mass of the central body, if the velocity on the surface of the object is the same as the velocity of the orbiting mass. The equatorial constraint of spin differs from orbits because of the null velocity along the special axis during spin. The absence of energy along the special axis is not accounted for in orbital models, which leads to excess mass and the inference of non-baryonic matter. Such matter has not been detected despite expenditures of billions of dollars over several decades, motivating alternative models [15,23–25,27–29]. Spin models give a reasonable mass for 14 large galaxies; see the table in [10]. Is this result general?

Many extractions of $v(r)$ from Doppler measurements exist, mostly on spirals. Lelli et al. [53] summarize the data on 175 spiral galaxies. Our companion paper lists data on 51 galaxies [40]. The list of Wiegert and English [51] covers non-interacting galaxies. A total of 356 galaxies have published RC curves, as well as distances and luminosity [33]. Figure 6 shows mass calculated from (1) using velocity at the visible edge from the original papers. The calculated value linearly correlates with luminosity in the visible for $n = 3/2$. The 1:1 correlation for well-characterized galaxies [10] holds for the entire RC data base. Figure 6 mostly shows spirals, but low brightness, edge-on and a few dwarf galaxies are included. These categories describe smaller galaxies: many of these types depart significantly from the trend, which is explained by their large uncertainties in luminosities, velocities and aspect ratios. An estimated uncertainty for the calculation and the measured luminosity of about $\pm 20\%$ is compatible with the spread around the 1:1 fit. A more detailed analysis, considering galactic type, statistics and other density distributions, will be presented elsewhere.
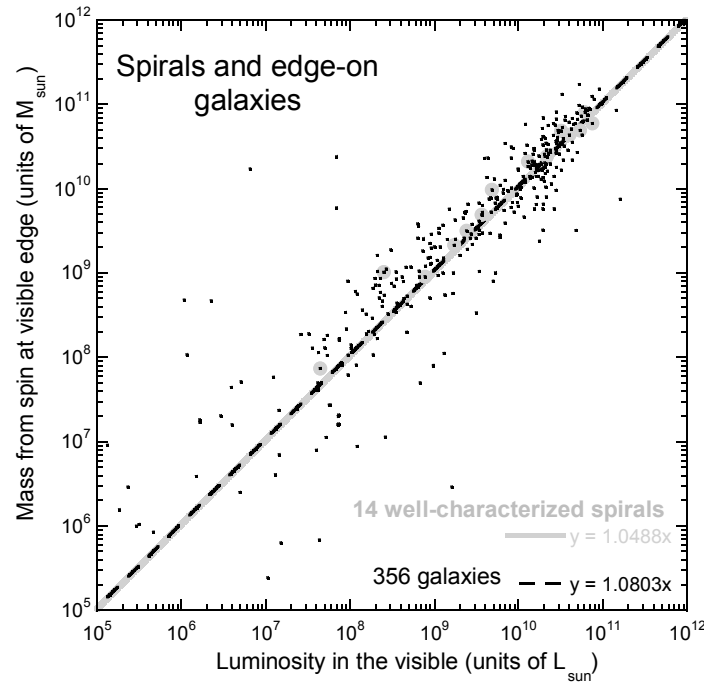
Figure 6. Comparison of calculated mass from Equation (1) to luminosity for all 356 galaxies with RC and luminosity data. Our model assumes coherent spin for a polytropic density function [10]. For consistency, luminosity, r_{edge} and aspect ratios were taken from [33]. Velocities at this radius were taken from the literature summarized in [41,53]. Typically, c/a ranged from 0.1 to 0.2. If the values were not reported, an average c/a of the edge-on galaxies was used.

Images (Figures 1 and 3) show that galaxies are spinning assemblies of gas and stars. Their mass from spin is compatible with their tangential velocity of spin (Figure 6). The observed correlation links the density distribution in spiral galaxies to a polytropic description of the precursor cloud of hydrogen gas. However, it must be recognized that differential spin exists. Thus, the index n does not need to exactly equal 3/2. Nonetheless, Figure 6 shows that the density distribution is similar for all spiral galaxies. These all formed in a similar manner and are all subject to the same forces. The correlation shows that non-baryonic matter is unnecessary to explain galactic dynamics.

3. Limitations in Applying Poisson's Equation

For any shape object, the theorem of Gauss connects the mass M_{in} enclosed in some surface of interest with the integral of the normal forces (F_{normal}) over this surface

$$\iint F_{normal} dS = -4\pi G M_{in} \tag{10}$$

where dS indicates a surface element. Note that the F_{normal} in (10) represents force on the affected particle per its unit mass, so F_{normal} is actually acceleration (e.g., [54]). The direct link of F_{normal} with interior mass is used here to specify how density in Poisson's equation must be computed for compliance with Newton's law.

Modern RC models do not actually use Poisson's equation, but instead have adopted a modified form proposed by [30], e.g., [17,55,56]:

$$-4\pi G \sum_{j} \rho_j(r) = \nabla^2 \psi \tag{11}$$

This formula from [30] is invalid.

First and foremost, the proposal of [30] is inconsistent with the well-known mathematics of partial differential equations. Addition of densities in (11) implies that solutions sum. Use of linear superposition is specifically stated in RC literature [55]. However, superposition (summing) is only appropriate for a homogeneous equation, which Poisson's equation most definitely is not [57]. The behavior of non-homogeneous partial different equations is very well known, and it is mathematically proven that solutions cannot be summed [57–59]. These proofs are not contestable, and all mass models using (11) are therefore invalid.

Second, a fundamental concept of classical thermodynamics is that intensive and extensive variables (properties of the system) behave in different, but specified ways [32,60]. Intensive variables such as temperature or refractive index do not sum, whereas extensive variables such as mass or energy do sum. Whether a variable is dependent or independent is distinct from these classifications [61]. The concept of intensive variables is essential to understanding components in a system and underlies J.W. Gibbs's circa 1878 phase rule and P. Duhem's theorem of 1898 [61]. For concreteness, we consider the thought experiment of tossing one gold coin into the Pacific Ocean: the summed densities are like gold, but the summed masses scarcely differ from that of the Pacific Ocean. Obviously, summing masses is germane, and the density summation of (11) that is ubiquitous in RC models is suspect.

Minimizing the dark matter component during fitting is needed to provide amounts of baryonic matter compatible with luminosity, e.g., [5,16,17,20]. The arbitrariness of this procedure proves that the density summation is problematic from a mathematical and physical viewpoint.

Third, the correct form for Poisson's equation, stated in terms of the spherical radius (s), is:

$$-4\pi G\rho(s) = \nabla^2\psi. \tag{12}$$

Equation (11), with a single density, is not equivalent to (12), as can be confirmed by transforming coordinates. In detail, from Equation (4), $\rho(s) = \rho_0 f(z)g(r)$, where f and g are some functions. This can be redefined as $\rho(s) = f(z)\rho(r)$, where f has no units. Thus, the correct mathematical form for (11), if densities actually could be summed, would be:

$$-4\pi G\sum_j f_j(z)\rho_j(r) = \nabla^2\psi$$

Dehnen and Binney [30] implicitly and erroneously assumed that density in the z direction is constant ($f = 1$).

Fourth, utilizing Poisson's Equation (12) requires that the interior (i.e., the object of interest) is distinct from its surroundings. If the problem to be addressed involves multiple masses, then the effect of their combined forces on some external test mass involves integrating over several surfaces and summing, as illustrated in Figure 2e. For RC, the problem is that both the mass inside (M_{in}) and mass outside some equatorial radius can affect the particle orbiting at that radius (Figure 2b), as shown by force models [27]. Unless the mass outside the radius of interest is distributed spherically, or spheroidally if rotating, it contributes a force in addition to that represented by (10) and must be considered with another surface and volume.

3.1. Derivation of Poisson's Equation from the Theorem of Gauss

The coordinate-free definition of the divergence [62] is:

$$\text{div}\,\vec{F} = \lim_{V\to 0}\left(\frac{1}{V}\iint F_{normal}dS\right) \tag{13}$$

where V is volume. Combining (10) and (13) gives:

$$\text{div}\,\vec{F} = \lim_{V\to 0}\left(\frac{-4\pi GM_{in}}{V}\right) = -4\pi G\lim_{V\to 0}\left(\frac{M_{in}}{V}\right). \tag{14}$$

Furthermore, $F = \nabla \psi$, where ψ is the potential emanating from the interior and is per the mass of an affected particle. There is no need to manipulate (14) further. We simply take the limit.

The existence of an interior mandates that an origin exists. The importance of this origin in applying Poisson's equation is understood by considering three simple cases that describe certain distributions of mass about an origin.

Case 1. For constant density, $\rho(r) = \rho_{in}$ = constant over the volume of interest, then the limit of (14) is obviously $-4\pi\rho_{in}G$, and large or small volumes pertain. Taking the gradient of (14) obviously produces (12), and (14) with this limit also reproduces Newton's law via integration.

Case 2. For a point mass at the origin, the limit of (14) is the density at the origin, $\rho(r = 0) = \rho_0$, which does not equal the density at some radius that is in reference to the origin, because $\rho(r > 0) = 0$. For this case, (12) is not reproduced. Yet, integration of (14) yields Newton's law.

Case 3. For a spherically-symmetric interior mass, neither volume, mass, nor density depend on the angular variables θ and ϕ, but each is only a function of s, the spherical radius. Then, $M_{in} = 4\pi \int_0^s q^2 \rho_{in}(q)dq$ and $V = 4\pi \int_0^s q^2 dq$ where q is a dummy variable. If one shrinks the volume around some arbitrary point, the density indeed becomes the density at that point; but, the potential that we wish to compute pertains to the mass about the origin, not the mass about some random point in space. Clearly, the limits of M_{in} and V cannot be taken separately. Instead, the limit must be taken of the ratio M_{in}/V:

$$\frac{M_{in}}{V} = \frac{\int_0^s \rho_{in}(q)q^2 dq}{\int_0^s q^2 dq} = \rho_{in,ave}(s) \tag{15}$$

The resulting limit of $\rho_{in,ave}(s)$ is valid for any s, regardless of whether the mass reaches s or not. An important example is a planet or star, where the density drops to zero or grades to zero at the outermost body radius, and the interest is the motion of some object at s that exceeds the body radius. If the mass does not reach s, then the average is lower than if the mass touches the radius of interest. Equation (12) with $\rho = \rho(s)$ is not general under spherical symmetry because $\rho_{in,ave}(s)$ does not equal $\rho(s)$ unless density is constant over the entire volume. Importantly, using (15) in (14) reproduces Newton's law, regardless of how density is specifically distributed with radius [2].

General case: We now consider a less regular interior mass distributed about a fixed origin. If θ (dummy variable θ') is the angle in the equatorial plane and ϕ (dummy variable ϕ') refers to the angle perpendicular to the plane and the object is symmetrical with respect to the plane, then by definition:

$$\frac{M_{in}}{V} = \frac{\int_0^s \int_0^\theta \int_{-\varphi}^\varphi q^2 \rho(q, \theta\prime, \varphi\prime) \sin(\varphi\prime)dqd\theta\prime d\varphi\prime}{\int_0^s \int_0^\theta \int_{-\varphi}^\varphi q^2 \sin(\varphi\prime)dqd\theta\prime d\varphi\prime} = \rho_{in,ave}(s, \theta, \varphi) \tag{16a}$$

Density being distributed with an angular dependence (e.g., cylinders or bicones) makes such integrations complicated, but the relevant density is still the average. For problems where density is not radially symmetric, the surface of choice may not be the sphere. For this situation, using the theorem of Gauss is more straightforward than using Poisson's equation. Nonetheless, Poisson's equation for a mass distribution about some origin and isolated in space under spherical-polar coordinates is:

$$-4\pi G\rho_{in,ave}(s, \theta, \varphi) = \nabla^2 \psi(s, \theta, \varphi), \tag{16b}$$

where the average is computed from (16a) in the spherical-polar coordinate system. If spherical symmetry exists, Newton's law is obtained. Again, if mass is distributed spherically outside, then the above holds.

If another coordinate system better describes the mass, then the average should be computed over the appropriately shaped volume, and the divergence involves the analogous coordinate system. For the case of axisymmetric geometry and an isolated mass, by definition:

$$\frac{M_{in}}{V} = \frac{\int_0^r \int_{-z}^z q\rho(q,u)dqdu}{\int_0^r \int_{-z}^z qdqdu} = \rho_{in,ave}(r,z) \tag{17a}$$

$$-4\pi G\rho_{in,ave}(r,z) = \nabla^2\psi(r,z), \tag{17b}$$

Due to the nature of the shape, both the r and z dependence of density must be specified. The condition of isolation is not needed if the exterior mass is distributed spheroidally and rotating. The complexity of (17) is consistent with the axisymmetric version of Poisson's equation being difficult to solve [63] even under constant density.

3.1.1. Previous Derivations

Previous derivations (e.g., [54]) manipulate the theorem of Gauss by first converting (10) to a volume integral, which provides $\int divFdV = -4\pi GM$, and then, allow the volume to shrink about a point, which provides div $F = -4\pi G\rho$, leading to (12). This approach only describes the field emanating from some tiny volume, which does not necessarily contain the origin, and further assumes no other mass exists, unless it is radially symmetric about that point. Errors in this approach are, first, that the limit is not taken of the ratio M_{in} over V, but of each independently, and second, that the connection of the potential with a specific origin is lost. Only for constant density is this approach valid.

3.1.2. Some Implications and an Example

Using Equation (11) in RC models thus sets two conditions. First, constant density for the interior is presumed, which is the source of overly large dynamical mass. Second, a line source of mass is presumed when z is neglected or small in order for forces in the plane to balance (detailed in Sections 3.3 and 3.4).

To again emphasize the importance of the central reference point (the origin), we compare the gravitational potential for the three-body problem [64] to the potential originating from the center of mass affecting a distant mass, m_4:

$$U_{g,3body} = -\frac{Gm_1m_2}{r_1 - r_2} - \frac{Gm_2m_3}{r_2 - r_3} - \frac{Gm_3m_1}{r_3 - r_1}; \; U_{g,external} = -\frac{G(m_1 + m_2 + m_3)m_4}{r_{center-m4}} \tag{18}$$

where subscripts 1–4 refer to individual masses and the distances are particle separations. Equation (18) (left) describes the interactions of the three masses: orbits in this system are unlike Keplerian [64,65]. Equation (18) (right) describes the effect of the configuration of stars in Figure 2e on a distant test mass, m_4, if the planet and moon masses are negligible compared to any star mass. (Equation (18), right) will provide a Keplerian orbit for m_4. However, Equation (18) (right) is only valid at large r.

The density term in Poisson's equation is associated with the average interior density. To drive this point home, the surface considered in (10) might involve a tiny mass with huge density that is distant from some large object surrounding the origin with much lower density. The force that is experienced by the tiny mass is not that associated with the high density at r, but is associated with the low density of the large mass enclosed in the volume of interest. In other words, the mass providing the field (M_{in}) is not identical to the mass subjected to the field (m). Hence, the density in Poisson's equation pertains to the interior in Gauss's theorem.

How the average of ρ_{in} should be calculated is not addressed by Poisson's Equation (16b), but is specified by a definition (16a). Additional information or constrains are needed. Using Poisson's equation requires many integrations, four to be precise. The theorem of Gauss, being already cast

in terms of mass, avoids the problem of integrating the density, and clearly distinguishes the object providing the force from the test mass subject to the force.

3.2. Internal (Self) vs. External Potentials

The fundamental solution of Poisson's equation in spherical coordinates is:

$$\psi = -\frac{GM_{\text{in}}}{s} \tag{19}$$

(see e.g., [66], which explains the connection of fundamental solutions with point masses at the origin). Hidden in the derivation is the requirement of spherical symmetry for mass or density. This result is per unit mass and is equivalent to the ordinary gravitational potential, which describes the attraction between a spherical or point mass M_{in} and an external point mass m:

$$U_{\text{g,external}} = -\frac{GM_{\text{in}}m}{s} \tag{20}$$

It is well known that the gravitational potential interior and exterior to an object differ [67,68]. Equation (18) provides one example of this difference. For emphasis, we now consider the simple case of a sphere whose density is described by a polytropic equation of state. This was derived by Emden [69] to model nebulae and rainclouds and was popularized by Eddington [70] through his models of stellar interiors. For constant density:

$$U_{\text{g,self}} = -\frac{3}{5}\frac{GM_{\text{in}}^2}{S} \tag{21}$$

where S is the body radius. The numerical factors and masses of (21) differ from (20), as they must because the gravitational potential inside an object describes all interactions between all particles [67]. Use of exterior potentials in RC models leads to excessive mass.

Maclaurin evaluated the double integral of (9) for the oblate spheroid. The result [42] is simple for homogeneous density:

$$U_{\text{g,self,oblate,h}} = -\frac{3}{5}\left(1 - e^2\right)^{\frac{1}{6}}\frac{\arcsin(e)}{e}\frac{GM_{\text{in}}^2}{a} \tag{22}$$

Using (21) in the Virial theorem provides spin periods that are consistent with rapid spin being observed for young stars [39]. Applying (22) to galactic spin provides total mass (in terms of suns) within the visual radius that match the luminosity from that region [10] (in terms of suns, Figure 6), whereas considering differential rotation yields densities vs. r that are compatible with astronomical environments [40].

3.3. Logarithmic Solutions to Poisson's Equation Require the Line Source

Modelling galactic disks in cylindrical coordinates (r, z) has led to many potential functions with logarithmic forms (e.g., Table 1 in [6]). For example,

$$\psi_{\text{EB}}(r, z) = -\frac{GM}{a}\log\left[a + \sqrt{b^2 + z^2} + \sqrt{\left(a + \sqrt{b^2 + z^2}\right)^2 + r^2}\right] \tag{23}$$

where the parameters are restricted to $a + b > 0$ with $b > 0$ and thus $a > 0$ [6]. The dependence of velocity on radius for relatively large r is particularly important to RC because this controls the amount of dark matter. However, (23) does not reduce to the correct limit of Equation (19) for orbits at very large r (and $z = 0$), far beyond RC measurements, that are associated with a massive central point and Newton's law.

The correct limit for a point source is not provided in RC models because cylindrical coordinates actually describe a line source when only the *r* dependence is considered (Figure 2d). Elementary physics textbooks provide a mathematical analysis of the analogous problem of describing the electric field around a line of charge [2]. This conclusion can also be reached by considering the shape of the volume element (Figures 3f and 4d), which remains cylindrical as *r* shrinks, while *z* is unchanged, and the requirement of Poisson's equation that the surface encloses a three-dimensional volume. This conclusion is also evident in (17a),(17b).

3.4. Thin Disks

Many papers on galactic rotation view spiral galaxies as thin disks [6]. It is valid to use this approximation in force calculations of distributions [27–29], but applying Poisson's equation to the equatorial plane is invalid, because this surface does not enclose a volume, e.g., [54].

Applying Poisson's equation to the equatorial plane within a rotating galaxy differs in a subtle way. This approach implicitly assumes infinitely tall cylinders and an infinitely tall line mass source along the *z* axis. The moment of inertia for the point mass is the same for a tall cylinder. Furthermore the density as a function of *z* does not enter directly into the fitting, but as used in existing RC models, provides one unconstrained free parameter for each postulated, non-spherical mass component. Good fits obtained in RC models are predicated on incorrect physics.

4. Vertical Gravitational Instability Inherent to Cylindrical Coordinates

The oblate spheroid is gravitationally stable, so that $v(z) = 0$ at any point. Tangential velocity at a general point is complicated, but the angular velocity of every homeoidal shell is constant, even during differential rotation, because these are equipotential (Newton's homeoid theorem; also see [40]). Thus, given a measured RC, one can use (2) to establish angular velocity anywhere, from the coordinate point and the velocity at the intercept of the relevant homeoidal shell on the radial plane.

Other shapes can be analyzed. These are unstable and will have vertical velocities and accelerations. The theorem of Gauss is simple for cylindrical coordinates when radial symmetry exists, because the relevant normal forces are orthogonal. For example, for the cylinder, F_z acts on only the top and bottom faces, while F_r acts only on the cylinder walls. Accounting for F_z above the equatorial plane pointing in the negative direction and conversely, we simplify (10) to provide positive, scalar mass:

$$4\pi \int_0^a F_z(r, b) r \, dr + 2\pi a \int_{-b}^b F_r(a, z) \, dz = 4\pi G M_{in} \tag{24}$$

where *a* and *b* represent disk radius and height. Simplifying (24) gives:

$$\frac{1}{a} \int_0^a F_z(r, b) r \, dr + \int_0^b F_r(a, z) \, dz = \frac{G M_{in}}{a} \tag{25}$$

This simplicity permits evaluating vertical instability. We provide approximate relationships in order to understand the general behavior.

4.1. Instability of the Thin Disk: A First Approximation

Coin-like shapes underlying RC models are highly amenable to analysis. For a relatively thin disk, F_r should not depend strongly on *z*, permitting further simplification of (25) to:

$$\frac{1}{a} \int_0^a F_z(r, b) r \, dr + b F_r(a) = \frac{G M_{in}}{a} \tag{26}$$

If the disk is rotating, then centrifugal force should balance gravitational pull. Roughly, but not exactly, $F_r = GM_{in}/a^2 = v^2_{edge}/a$ since b/a is small. No such balance exists in the z direction. Equation (26) becomes:

$$\frac{1}{a}\int_0^a F_z(r,b)r dr = \frac{GM_{in}}{a}\left(1 - \frac{b}{a}\right) \sim v_{edge}{}^2. \tag{27}$$

As a first approximation, we consider a rough average for F_z:

$$\frac{a}{2}F_{z,average} = \frac{GM_{in}}{a}\left(1 - \frac{b}{a}\right) \sim v^2_{edge}. \tag{28}$$

Equation (28) actually depicts acceleration because F is defined per mass of the test particle. Hence,

$$\frac{dv_{z,average}}{dt} \cong 2\frac{v^2_{edge}}{a}. \tag{29}$$

To simplify (29), we assume that $v_{z,average} = 0$ at $t = 0$, integrate and recognize that $2\pi a/\text{period} = v_{edge}$. Furthermore, let $t = n \times \text{period}$, where n can be a fraction of a revolution or a multiple, giving:

$$v_{z,average} \cong 2\frac{v^2_{edge}}{a}t = 4\pi n v_{edge}. \tag{30}$$

Thus, within some fraction of a revolution, the average velocity in z exceeds the tangential velocity at the edge. Collapse occurs, roughly, before a thin disk-shaped galaxy can complete a revolution. The coin-like shape is highly unstable due to the decoupling of the vertical from the radial forces and to the axial rotation (spin) providing opposition only in the radial direction.

4.2. Vertical Instability of the Disk in Analytical Models of RC

Evans and Bowden [6] provide an analytical form for the unopposed force in the z-direction. Although they considered orbits, not spin, their result is illuminating. Since their force is per mass, the vertical acceleration is actually provided. Towards the plane:

$$\frac{\partial v_z}{\partial t} = \frac{zv_0^2}{\sqrt{z^2 + b^2}\sqrt{r^2 + \left(a + \sqrt{z^2 + b^2}\right)^2}} \approx \frac{v_0^2}{2a} \tag{31}$$

where $v_0{}^2 = GM_{dyn}/a$ is tangential v_r associated with the point mass limit of (7). The RHS approximation assumed a flat disk ($b/a < 0.1$) and considers the upper surface ($z = b$) and $r \sim a$, where $v_r \sim v_0$. We integrate (31) assuming stationary faces at time $t = 0$. The RHS provides:

$$v_z \cong \frac{v_0^2}{2a}t = v_0\pi n. \tag{32}$$

The RHS of (32) uses the fact that time is proportional to the period of galactic rotation: $t \sim n2\pi a/v_0$, where n is the number of revolutions. Thus, before the galaxy completes a single revolution, v_z near the edge exceeds v_0. Because $b < a$, the disk corners will collapse before even one revolution is completed, as above. Repeating this exercise for $r = 0$ and $z = b$ gives larger $v_z \sim v_0{}^2 t/(a\sqrt{2})$. The faces collapse faster at their centers because these are closer to the center of mass. Note that provision of a bow-tie profile, rather than the oblate, is caused by [6] considering orbits, not spin.

No evidence suggests that large vertical velocities exist in galaxies. Interestingly, our analysis suggests that a rotating disk-shaped galaxy cannot exist, unless it is infinitesimally thin, or infinitely tall. The underlying problem is that neither the hollow pillbox, nor bicone shapes, defined by density variations in a cylindrical system, can be equipotential surfaces under Newtonian physics.

5. Triggered Collapse of Nebulae to Form Planar Systems

The similarly flat shapes of the Solar System and spiral galaxies suggest commonalities exist in their formation mechanisms. We therefore discuss the formation of the Solar System, where more information is available to evaluate such models.

Popular models of the formation of the Solar System involve fractal assembly of increasingly larger objects through energetic, high speed (>km/s) collisions, which oddly are assumed to be constructive [71–73]. Fractal models do not conserve angular momentum, do not address how small particles of dust coagulate and do not explain how ballistic impacts, which are destructive in nature, result in planetary growth. Neither do these models explain observed regularities such as orientation and handedness in axial spin and why planar orbital motions are circular and concentric. The models are motivated by the scarred surfaces of planets and moons, but these features bear witness to multiple impacts that occurred during the final stages of accretion, not to the early stages when the bodies formed and grew.

Conservative formation of the Solar System from the collapse of a dusty gas cloud explains the regularities in planetary spin and orbits [38]. Incorporating the Virial Theorem of Clausius further restricts energies, reducing the axial spin energy by a factor of $\frac{1}{2}$, which provides better agreement with the spin of young stars [39]. This model is based on the well-known conversion of potential to kinetic energy [2], which is followed by time-dependent heating when the motions involve friction. The planar geometry of the Solar System was proposed to occur as "pancaking," i.e., vertical collapse of the spinning nebula. The mechanism tentatively offered [38] to explain the vertical nature of the collapse that formed the dusty planets, as opposed to contraction about a point, which formed the gassy Sun, was dust particle collisions. Contractive collapse was discussed in terms of the stability of the nebulae, whereby thermal kinetic motions oppose the gravitational inward pull. Because thermodynamic principles show that either cooling of the nebulae or injection of mass will cause contraction, we used the time-dependent Virial theorem to explore the collapse. However, this formulation contains errors [39], and hence, the vertical and catastrophic nature of nebular collapse warrants further exploration.

A stably-spinning nebula, no matter how large, must have an equilibrium shape: Maclaurin's oblate spheroid describes the shape accompanying slow rotation. If an injection occurs, as suggested by chemical compositions of planetary material, which further accounts for short-lived isotopes [74], not only is the mass increased, which affects the thermal-kinetic and gravitational balance [38], but the shape is altered, which affects the rotational and gravitational balance. Gravitational forces changing in the radial direction can be accommodated by changes in rotational velocity, but changes of gravitational forces in the azimuthal direction are essentially unopposed, therefore triggering vertical contraction (Section 4). Because the process involves rapid velocities, as shown above, vertical collapse occurs within a short period of time and forms a plane with the sense of nebular rotation and velocities preserved in the planetary orbits.

Nebulae are inherently instable because these lack a containing surface, and so molecules that have higher kinetic energy than the average can diffuse out [38]. If the oblate shape is maintained while the hot molecules leave, the cloud shrinks as it cools and spins up as potential energy is converted to kinetic energy. The temperature of the cloud depends on a radiative balance between incoming light from stars and losses of heat due to diffusion of photons and hot molecules. If the incoming radiation and/or the losses alter the equilibrium shape, vertical collapse will occur. As discussed previously [38], dust particles and molecules, as well as ices, are heavy and slow moving and are more prone to collapse than the low mass, energetic H_2 and He molecules. Thus, dust and ice constituents cause a disk that is dustier than the remaining 3D nebulae to form first by collapse. The contraction that follows this collapse is to the center, as required by Newton's law, thereby yielding the Sun.

The flat forms of spiral galaxies, which are young, are consistent with vertical collapse of a much, much larger cloud of gas and dust than that of the presolar nebula associated with our Solar System. The process of collapse and evolution is slow, due to the great distances involved, providing complexity

beyond that present in our simple Solar System. Importantly, because galactic processes are slow and occur over enormous scales, the equilibrium oblate shape closely resembles spiral galaxies. Departures from that shape yield superimposed details (bulge, rings and arms), which create the beauty and variety of galactic images [33].

6. Conclusions

From textbook resources and analytical mathematics, we have demonstrated that mainstream models of galactic rotation curves are inconsistent with the theorem of Gauss, Newton's homeoid theorem, geometrical constraints, and mathematical techniques used to solve Poisson's and similar equations. Their errors in mathematical physics are summarized as follows:

- Use of the cylindrical coordinate system to model RC implicitly assumes that an infinite line of mass exists along z at $r = 0$. The large inferred mass of non-baryonic matter is closely connected with the required, but unrealistic, line source.

- Decoupling density in the z and r directions induces one unconstrained parameter in the fitting models for each of several postulated mass components. Hence, "good" fits to rotation curves involve several free parameters and do not validate RC fitting models.

- Because the calculated orbits in the equatorial plane do not account for orbital dependence on z, a hidden assumption in RC models is that rotating concentric cylinders describe galactic motions. Therefore, the assumed shape is implicitly the tall cylinder, not the flat coin.

- Density functions assumed in RC models conform to neither cylindrical, nor oblate spheroidal shapes, whereas the latter closely resembles spiral galaxies. The shapes implied by the assumed density functions are further inconsistent with the assumed moment of inertia.

- Instability exists in all RC models because the assumed isodensity surfaces are not equipotential, except in the spinning, oblate spheroid. We considered vertical stability and showed that this effect is huge. We estimate that vertical collapse would occur within about one galactic revolution.

- Because orbits are considered, neither the mass, nor density at the radius of interest are constrained.

- Importantly, Poisson's equation is not actually used: instead the erroneous modification from [30] is employed. Referring to Poisson's equation as the basis of RC analysis conceals the above problems. This equation describes the potential emanating from the object. Limitations that accompany use of Poisson's equation in any application are summarized as follows:

- The potential must be computed by integrating density with respect to some specific origin, to describe how the mass around that origin affects a test particle at a distance. It is implicitly assumed that either the object is isolated, or that any mass located outside the surface is spherically distributed (if not spinning), or uniformly distributed in each shell of an oblate spheroid (if spinning).

- The density in Poisson's equation refers to that of the interior, not ρ at the radius of interest. Equation (16b) presents a revised Poisson's equation with average density defined in (16a) for spherical-polar coordinates. Equation (17ab) concerns cylindrical shapes and coordinates.

- As is well known, the surface of interest must enclose a finite volume, and thus, Poisson's equation is inapplicable to the equatorial plane and to thin disks. Any such use in astrophysical problems is either invalid or implicitly assumes an infinite line source of mass along the z axis.

As regards application to RC of galaxies, multiple errors have led to overestimating mass, confusing radial with spherical symmetry (see Equations (11) and (12)), and erroneously superimposing solutions via a questionable density summation. Errors in mathematical physics are the source of the unconfirmed hypothesis that huge halos of dark matter surround spiral galaxies.

In general, symmetry provides an important constraint on the mathematical analysis of periodic motions in 3D space, as is known for orbital motions [39] and for vibrations [1]. Our results suggest utilizing symmetry may permit exploring periodic motions in spacetime geometries. Poisson's

equation is limited to the effect of M_{in} inside some volume on some exterior mass that is not included in this volume. This stipulation has multiple repercussions on problems of astronomical and planetary interest regulated by Newton's law in Euclidian geometry. Our findings also apply to motions on any scale. One example is that Earth's outermost layers are not spherically symmetric because huge, dense tectonic plates descend to great depths. Inverse models of Earth's internal structure based on Poisson's equation may be perturbed by this asymmetry. Furthermore, these applications need to be revised so that the requisite average density is utilized.

In problems of rotation coupled with gravitation, the theorem of Gauss has many advantages over Poisson's equation, since the former directly specifies interior mass.

Author Contributions: A.M.H. wrote the paper. The ideas and presentation evolved through an integrated effort with R.E.C.

Conflicts of Interest: The authors declare no conflict of interest.

References and Note

1. Cotton, F.A. *Chemical Applications of Group Theory*; Wiley-Interscience: New York, NY, USA, 1963.
2. Halliday, D.; Resnick, R. *Physics*; John Wiley and Sons: New York, NY, USA, 1966.
3. Binney, J.; Tremaine, S. *Galactic Dynamics*, 2nd ed.; Princeton University Press: Princeton, NJ, USA, 2008.
4. Bertin, G. *Dynamics of Galaxies*, 2nd ed.; Cambridge University Press: Cambridge, UK, 2014.
5. Sofue, Y.; Rubin, V.C. Rotation curves of spiral galaxies. *Ann. Rev. Astron. Astrophys.* **2001**, *39*, 137–174. [CrossRef]
6. Evans, N.W.; Bowden, A. Extremely flat halos and the shape of the galaxy. *Mon. Not. R. Astron. Soc.* **2014**, *43*, 2–11. [CrossRef]
7. Sofue, Y. Dark halos of M 31 and the Milky Way. *Publ. Astron. Soc. Jpn.* **2015**, *67*, 759. [CrossRef]
8. Bottema, R.; Pestaña, J.L.G. The distribution of dark and luminous matter inferred from extended rotation curves. *Mon. Not. R. Astron. Soc.* **2015**, *448*, 2566–2593. [CrossRef]
9. Perek, L. Heterogeneous spheroids with Gaussian and exponential density laws. *Bull. Astron. Inst. Czechoslov.* **1958**, *9*, 208–212.
10. Hofmeister, A.M.; Criss, R.E. The physics of galactic spin. *Can. J. Phys.* **2017**, *95*, 156–166. [CrossRef]
11. Todhunter, I. *A History of the Mathematical Theories of Attraction and Figure of the Earth*; Dover Publications: New York, NY, USA, 1962.
12. Faber, S.M.; Gallagher, J.S. Masses and mass-to-light ratios of galaxies. *Ann. Rev. Astron. Astrophys.* **1979**, *17*, 135–187. [CrossRef]
13. Rubin, V.C.; Ford, W.K. Rotation of the Andromeda nebula from a spectroscopic survey of emission regions. *Astrophys. J.* **1970**, *159*, 379. [CrossRef]
14. Ackermann, M.; Albert, A.; Anderson, B.; Baldini, L.; Ballet, J.; Barbiellini, G.; Bastieri, D.; Bechtol, K.; Bellazzini, R.; Bissaldi, E.; et al. Dark matter constraints from observations of 25 Milky Way satellite galaxies with the Fermi Large Area Telescope. *Phys. Rev. D* **2014**, *89*, 042001. [CrossRef]
15. Brownstein, J.R.; Moffat, J.W. Galaxy rotation curves without nonbaryonic dark matter. *Astrophys. J.* **2006**, *636*, 721–741. [CrossRef]
16. Kam, Z.S.; Carignan, C.; Chemin, L.; Amram, P.; Epinat, B. Kinematics and mass modelling of M33, Hα observations. *Mon. Not. R. Astron. Soc.* **2015**, *449*, 4048–4070. [CrossRef]
17. Ibata, R.; Lewis, G.F.; Martin, N.F.; Bellazzini, M.; Correnti, M. Does the sagittarius stream constrain the milky way halo to be triaxial? *Astrophys. J. Lett.* **2013**, *765*, L155. [CrossRef]
18. De Vega, H.J.; Salucci, P.; Sanchez, N.G. Observational rotation curves and density profiles versus the Thomas-Fermi galaxy structure theory. *Mon. Not. R. Astron. Soc.* **2014**, *442*, 2717–2727. [CrossRef]
19. Ade, P.A.R.; Aghanim, N.; Armitage-Caplan, C.; Arnaud, M.; Ashdown, M.; Atrio-Barandela, F.; Aumont, J.; Baccigalupi, C.; Banday, A.J.; Barreiro, R.B.; et al. Planck 2013 results. XVI. Cosmological parameters. *Astron. Astrophys.* **2014**, *571*, A16.

20.   Gentile, G.; Salucci, P.; Klein, U.; Vergani, D.; Kalberla, P. Mapping the inner regions of the polar disk galaxy NGC 4650A with MUSE. *Mon. Not. R. Astron. Soc.* **2004**, *351*, 903. [CrossRef]

21.   Disney, M.J. Modern Cosmology, Science or Folktale? *Am. Sci.* **2007**, *95*, 383–385.

22.   Transtrum, M.K.; Machta, B.B.; Brown, K.S.; Daniels, B.C.; Myers, C.R.; Sethna, J.P. Perspective: Sloppiness and emergent theories in physics, biology, and beyond. *J. Chem. Phys.* **2015**, *143*, 010901. [CrossRef] [PubMed]

23.   McGaugh, S.S. A tale of two paradigms, the mutual incommensurability of LCDM and MOND. *Can. J. Phys.* **2015**, *93*, 250–259. [CrossRef]

24.   Milgrom, M. A modification of the Newtonian dynamics as a possible alternative to the hidden mass hypothesis. *Astrophys. J.* **1983**, *270*, 365–370. [CrossRef]

25.   Lin, H.-N.; Li, M.-H.; Li, X.; Chang, Z. Galaxy rotation curves in the Grumiller's modified gravity. *Mon. Not. R. Astron. Soc.* **2013**, *430*, 450–458. [CrossRef]

26.   Clemence, G.M. The Relativity Effect in Planetary Motions. *Rev. Mod. Phys.* **1947**, *19*, 361. [CrossRef]

27.   Feng, J.Q.; Gallo, C.F. Mass distribution in rotating thin-disk galaxies according to Newtonian dynamics. *Galaxies* **2014**, *2*, 199–222. [CrossRef]

28.   Pavlovich, K.; Pavlovich, A.; Sipols, A. Newtonian explanation of galaxy rotation curves based on distribution of baryonic matter. *arXiv* **2014**, arXiv:1406.2401P.

29.   Marr, J.H. Galaxy rotation curves with lognormal density distribution. *Mon. Not. R. Astron. Soc.* **2015**, *448*, 3229–3241. [CrossRef]

30.   Dehnen, W.; Binney, J. Mass models of the Milky Way. *Mon. Not. R. Astron. Soc.* **1998**, *294*, 429. [CrossRef]

31.   Moulton, F.R. *An Introduction to Celestial Mechanics*; MacMillan: New York, NY, USA, 1914.

32.   Maron, S.H.; Prutton, C.F. *Fundamental Principles of Physical Chemistry*; Macmillan: New York, NY, USA, 1970.

33.   NASA/IPAC Extragalactic Database. Available online: https://ned.ipac.caltech.edu/ (accessed on 10 May 2017).

34.   Dima, I.; Desflots, M. Wind Profiles in Parametric Hurricane Models; Report to Air Worldwide. 2010. Available online: www.air-worldwide.com/.../AIRCurrents-Wind-Profiles-in-Parametric-Hurricane-Models (accessed on 4 July 2017).

35.   Willoughby, H.E.; Darling, R.W.R.; Rahn, M.E. Parametric representation of the primary Hurricane vortex. Part II: A new family of sectionnally continuous profiles. *Mon. Wea. Rev.* **2006**, *134*, 1102–1120. [CrossRef]

36.   Sofue, Y.; Tutui, Y.; Honma, M.; Tomita, A.; Takamiya, T.; Koda, J.; Takeda, Y. Central rotation curves of spiral galaxies. *Astrophys. J.* **1999**, *523*, 136. [CrossRef]

37.   Sofue, Y.; Koda, J.; Nakanishi, H.; Onodera, S. The Virgo high-resolution CO survey, II. Rotation curves and dynamical mass distributions. *Publ. Astron. Soc. Jpn.* **2003**, *55*, 59–74. [CrossRef]

38.   Hofmeister, A.M.; Criss, R.E. A thermodynamic model for formation of the Solar System via 3-dimensional collapse of the dusty nebula. *Planet. Space Sci.* **2012**, *62*, 111–131. [CrossRef]

39.   Hofmeister, A.M.; Criss, R.E. Spatial and symmetry constraints as the basis of the virial theorem and astrophysical implications. *Can. J. Phys.* **2016**, *94*, 380–388. [CrossRef]

40.   Criss, R.E.; Hofmeister, A.M. Newtonian analysis of oblate spheroidal mass distributions: Inverse models of galactic rotation and determination of density distributions. *Res. Astron. Astrophys.* **2017**, in review.

41.   Hofmeister, A.M.; Criss, R.E.; Criss, E.M. Verified solutions for the gravitational attraction to an oblate spheroid: Implications for planet mass and satellite orbits. *Planet. Space Sci.* **2017**, in review.

42.   Dankova, T.; Rosensteel, G. Triaxial bifurcations of rapidly rotating spheroids. *Am. J. Phys.* **1998**, *66*, 1095. [CrossRef]

43.   Wiegert, T.; Irwin, J.; Miskolczi, A.; Schmidt, P.; Carolina Mora, S.; Damas-Segovia, A.; Stein, Y.; English, J.; Rand, R.J.; Santistevan, I. Changes in Radio continuum emission of 35 edge-on galaxies observed with the Karl G. Jansky very large array in D configuration—Data release 1. *Astronom. J.* **2015**, *150*, 81. [CrossRef]

44.   Schmidt, M. A model of the distribution of mass in the galactic system. *Bul. Astron. Inst. Neth.* **1956**, *13*, 15.

45.   Boroson, T. The distribution of luminosity in spiral galaxies. *Astrophys. J. Suppl.* **1981**, *46*, 177–209. [CrossRef]

46.   Freeman, K.C. On the Disks of Spiral and S0 Galaxies. *Astrophys. J.* **1970**, *160*, 811. [CrossRef]

47.   Sackett, P.D.; Sparke, L.S. The dark halo of the polarring galaxy NGC 4650A. *Astrophys. J.* **1990**, *361*, 408–418. [CrossRef]

48.   Van der Kruit, P.C.; Shostak, G.S. Vertical motion and the thickness of HI disks—Implications for galactic mass models. In *Internal Kinematics and Dynamics of Galaxies*; Athanassoula, E., Ed.; Kluwer: Boston, MA, USA, 1983; pp. 69–76.

49. Jardel, J.R.; Gebhardt, K.; Shen, J.; Fisher, D.B.; Kormendy, J.; Kinzler, J.; Lauer, T.R.; Richstone, D.; Gültekin, K. Orbit-based dynamical models of the Sombrero galaxy (NGC 4594). *Astrophys. J.* **2011**, *739*, 21. [CrossRef]

50. De Blok, W.J.G.; Walter, F.; Brinks, E.; Trachternach, C.; Oh, S.-H.; Kennicutt, R.C., Jr. High-resolution rotation curves and galaxy mass models from THINGS. *Astrophys. J.* **2008**, *136*, 2648. [CrossRef]

51. Wiegert, T.; English, J. Kinematic classification of non-interacting spiral galaxies. *New Astron.* **2014**, *26*, 40–61. [CrossRef]

52. Diaz, R.A.; Herrera, W.J.; Martinez, R. Moments of inertia for solids of revolution and variational methods. *Eur. J. Phys.* **2006**, *27*, 183–192. [CrossRef]

53. Lelli, F.; McGaugh, S.S.; Schombert, J.M. SPARC: Mass models for 175 galaxies with Spitzer photometry and accurate rotation curves. *Astrom. J.* **2016**, *152*, 157. [CrossRef]

54. Garland, G.D. *The Earth's Shape and Gravity*; Pergamon Press: Oxford, UK, 1977.

55. Chemin, L.; Huré, J.-M.; Soubiran, C.; Zibetti, S.; Charlot, S.; Kawata, D. Asymmetric mass models of disk galaxies—I. Messier 99. *Astron. Astrophys.* **2016**, *588*, A48. [CrossRef]

56. Two approaches are described in recent studies. Sofue (Ref. [7]) computes mass from assumed density functions and sums the masses in accord with the Keplerian balance of forces in Equation (7), which presumes incorrectly that the reduced 2-body problem holds for a galaxy. Most authors (Kam et al., Ref. [16]; Chemin et al., Ref. [55]) used density to compute potentials, infer a gravitational force, use a balance with centrifugal forces to compute velocities and then sum these velocities. This procedure is equivalent to applying the superposition principle to Poisson's equation. Other papers directly state that superposition (i.e., Equation (11)) is used (e.g., Ibata et al., Ref. [17]). Superposition appears to have originated in the 1990s, with Ref. [30].

57. Pinsky, M.A. *Introduction to Partial Differential Equations*; McGraw-Hill: New York, NY, USA, 1984.

58. Pivato, M. *Linear Partial Differential Equations and Fourier Theory*; Cambridge University Press: Cambridge, UK, 2010.

59. Hiraski, G.J. Lecture Notes for Transport Phenomena I Fluid Dynamics. Chapter 7 Covers Poisson's Equation in Detail. Available online: http://www.owlnet.rice.edu/~ceng501/ (accessed on 27 September 2017).

60. Nordstrom, D.K.; Munoz, J.L. *Geochemical Thermodynamics*; Blackwell Scientific: Palo Alto, CA, USA, 1986.

61. Prigogine, I.; Defay, R. *Chemical Thermodynamics*; Everett, D.H., Ed.; Longmans, Green, and Co.: London, UK, 1954.

62. Rojansky, V. *Electromagnetic Fields and Waves*; Prentice-Hall, Inc.: Englewood Cliffs, NJ, USA, 1971.

63. Chen, C.S.; Muleshkov, A.S.; Golbergy, M.A.; Mattheij, R.M.M. A mesh free approach to solving the axisymmetric Poisson's equation. *Numer. Methods Partial Differ. Equ.* **2005**, *21*, 349–367. [CrossRef]

64. Valtonen, M.; Karttunen, H. *The Three Body Problem*; Cambridge U. Press: Cambridge, UK, 2005.

65. Šuvakov, M.; Dmitrišinović, V. Three classes of Newtonian three-body planar periodic orbits. *Phys. Rev. Lett.* **2003**, *110*, 114301. [CrossRef] [PubMed]

66. Faris, W.G. Eprint, Lecture Notes on Partial Differential Equations. 1999. Available online: http://math.arizona.edu/~faris/lecturenotes.html (accessed on 4 July 2017).

67. Kellogg, O.D. *Foundations of Potential Theory*; Dover Publications: New York, NY, USA, 1953.

68. McCarthy, J.E.; Backhaus, E.; Fajans, J.Y. Solving Poisson's equation with interior conditions. *J. Math. Phys.* **1998**, *39*, 6720–6729. [CrossRef]

69. Emden, R. *Gaskuglen—Anwendungen de Mechanischen Wärmetheorie*; B.G. Teubner: Leipzig, Germany, 1907.

70. Eddington, A.S. *The Internal Constitution of Stars*; Cambridge U. Press: Cambridge, UK, 1926.

71. Safronov, V.S. *Evolution of the Protoplanetary Cloud and Formation of the Earth and Planets*; (Nauka, Moscow 1969: Translated by the Israel Program for Scientific Translations; NASA TT-677); Keter Publishing House: Jerusalem, Israel, 1972.

72. Kenyon, S.J.; Bromley, B.C. Terrestrial planet formation. *Astron. J.* **2006**, *131*, 1837. [CrossRef]

73. Armitage, P.J. Dynamics of Protoplanetary Disks. *Ann. Rev. Astron. Astrophys.* **2011**, *49*, 195–236. [CrossRef]

74. Hofmeister, A.M.; Criss, R.E. Origin of HED meteorites from the spalling of Mercury: Implications for the formation and composition of the inner planets. In *New Achievements in Geoscience*; Hwee-San, L., Ed.; InTech: Rijeka, Croatia, 2012; pp. 153–178.